Original Paper

phys. stat. sol. (a) **204**, No. 6, 1665–1671 (2007) / **DOI** 10.1002/pssa.200675337

Spontaneous growth of uniformly distributed In nanodots and InI_3 nanowires on InP induced by a focused ion beam

Victor Callegari[*] and **Philipp M. Nellen**

EMPA, Swiss Federal Laboratories for Materials Testing and Research, Ueberlandstr. 129, 8600 Duebendorf, Switzerland

Received 16 October 2006, revised 13 February 2007, accepted 16 February 2007
Published online 23 May 2007

PACS 61.80.Jh, 68.49.Sf, 68.65.Hb, 68.65.La, 81.05.Ea, 81.16.Rf

We show the growth of hemispherical In nanodots due to differential sputtering by 30 keV gallium (Ga^+) ions and of InI_3 nanodots and nanowires due to chemical reactions with iodine on the surface of focused ion beam-irradiated areas on a (100)InP substrate. Growth occurs exclusively on previously FIB-fabricated nucleation-sites in the form of craters and trenches. Surface topography and the native oxide on InP are identified as the factors determining the area of growth. Arbitrary 2D patterns can be generated with good control of localization and dimension of the nanostructures. Limitations of size and surface density of the nanodots and nanowires are discussed.

1 Introduction

Focused ion beam instruments (FIB) can be used both as top-down (patterning) and bottom-up structuring tools. Bottom-up applications include self-assembly at random or specific locations during or after ion irradiation. We report on FIB-fabricated nucleation sites on (100)InP for In nanodots and InI_3 nanodots as well as nanowires. The hemispherical nanodots and nanowires grow exclusively at previously irradiated areas, showing the applicability of FIB for nanopatterning. Nanostructures whose localization can be precisely controlled are interesting for nanoelectronics and photonics applications. InP is a direct-band-gap semiconductor frequently used for optoelectronics applications because of the width of its band gap, which generates photons in the suitable regime for quartz fibers in telecommunications [1]. Nano-crystallite growth on FIB irradiated areas has been shown for GaAs and InAs [2].

2 Experimental

We used a dual beam system (FEI Strata 235) with integrated scanning electron microscope (SEM), placed at an angle of 52° from the ion column. The acceleration voltage of Ga^+ was 30 kV. For the FEI Strata 235, the minimum beam diameter is specified to 7 nm for 1 pA current and 30 kV acceleration voltage. The ion beam was scanned in a serpentine pattern over a 10×10 μm square area in all experiments where the scanning strategy is not explicitly mentioned. The beam current was 305 pA and beam overlap was set to 50% to yield a homogeneous ion distribution. The beam dwell time was set to 1 μs per pixel. Unless otherwise noticed, all experiments were performed at room temperature.

A nozzle with a diameter of 500 μm can be inserted into the vacuum chamber 150 μm above the InP surface. Solid iodine is heated to 35 °C to increase the vapor pressure. If the valve separating the iodine

[*] Corresponding author: e-mail: victor.callegari@empa.ch

reservoir from the vacuum chamber is opened, the pressure inside the chamber rises from 4×10^{-6} mbar to 2×10^{-5} mbar after ~10 seconds.

A heating stage was used to liquefy In in the vacuum chamber. A NiCr–Ni thermocouple is in contact with the chromium-coated copper surface. Considering the good thermal conductivity of InP and the wafer thickness of 300 µm, we expect no significant temperature gradient in InP [1].

Atomic force microscope (AFM) measurements were performed on a Digital Instruments Nanoscope IV in contact mode at room temperature in air.

3 In nanoislands

Sputtering rates are material dependent. Therefore, as many III–V semiconductors, InP sputters non-congruently. Phosphorus (P) is sputtered faster than Indium (In), especially for sputtering at normal incidence [3]. From Eq. (1) [3], this can be attributed to the lower mass and lower surface binding energy of P. An indication of the lower surface binding energy is the fact that InP sublimes incongruently above 365 °C, with a preferential loss of P_2 [4].

X^{surf} is the surface concentration of P and In, respectively, X^{bulk} the bulk concentration, A the atomic mass, m a parameter depending on the ion energy and mass from the Sigmund theory [5] ($m \approx 1/3$ for heavy ions and 30 kV) and U the surface binding energies of P and In in InP.

$$\frac{X_{\mathrm{P}}^{\mathrm{surf}}}{X_{\mathrm{In}}^{\mathrm{surf}}} = \frac{X_{\mathrm{P}}^{\mathrm{bulk}}}{X_{\mathrm{In}}^{\mathrm{bulk}}} \left(\frac{A_{\mathrm{P}}}{A_{\mathrm{In}}}\right)^{2m} \left(\frac{U_{\mathrm{P}}^{\mathrm{InP}}}{U_{\mathrm{In}}^{\mathrm{InP}}}\right)^{1-2m} . \tag{1}$$

According to Eq. (1), InP becomes In-rich under ion irradiation at room temperature. The excess quantity of In on the InP surface depends on the ion fluence. Indium tends to aggregate and form nanodots or islands, as shown in Fig. 1. The average size of these islands increases with increasing ion fluence and temperature (Fig. 2). As the size of the dots increases, the surface density of the islands decreases, a direct consequence of Ostwald ripening [6]. Surface density of the dots for a Ga fluence of 8.7×10^{15} cm^{-2} was determined from AFM measurements and is 2×10^{10} cm^{-2} (Fig. 1). For this fluence the irradiated surface receded 150 nm with respect to the unirradiated InP surface due to sputtering of InP. Typical dimensions of an In island for that ion fluence are 42 nm diameter and 7 nm height. The diameter is smaller than the reported diameter of 120 nm for Ga islands on GaAs [7]. This difference can be ex-

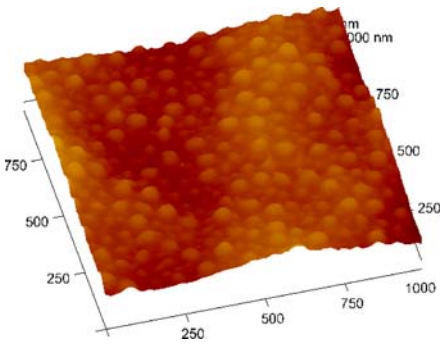

Fig. 1 (online colour at: www.pss-a.com) AFM image of the as-sputtered InP surface, showing the spontaneous growth of In nanodots under ion beam irradiation. The density of the dots is 2×10^{10} cm^{-2} for an ion fluence of 8.7×10^{15} cm^{-2} at RT.

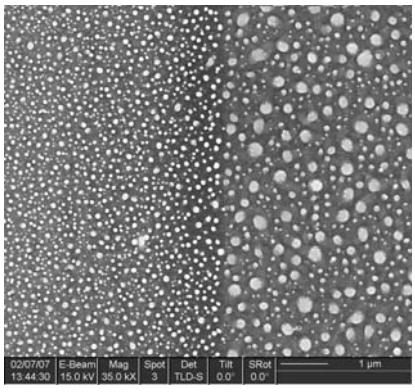

Fig. 2 SEM picture showing that the island-size and -density depend on the ion fluence (8.7×10^{15} cm^{-2} on the left hand side and 1.7×10^{16} cm^{-2} on the right). Stage temperature was 200 °C.

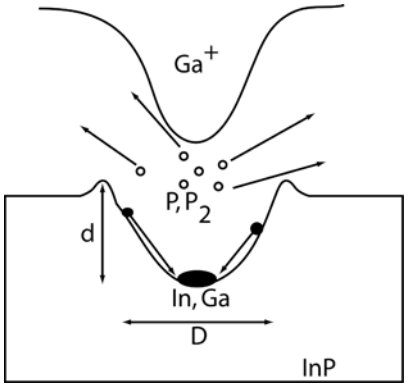

Fig. 3 Illustration of the InP sputtering process. Phosphorus is sputtered preferentially, leaving heavier In on the InP surface. Irradiation-enhanced diffusion might occur, leading to ripening in the crater. The crater depth d and diameter D depend on the ion distribution (shown here as Gaussian) and fluence.

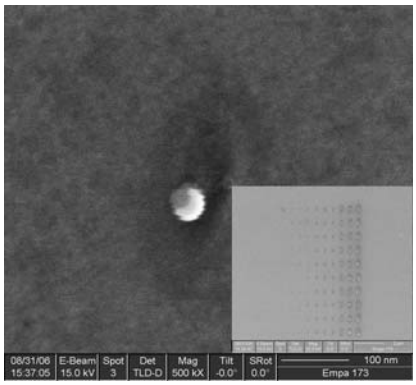

Fig. 4 SEM micrographs of a 40 nm diameter In island grown on a FIB-irradiated site at 200 °C stage temperature. Inset shows periodically ordered In nanodots.

plained by the fact that Ga is liquid under ion bombardment and ripening of the dots is enhanced by Ga diffusion on the surface. Metallic In has a melting temperature of 157 °C and melting of In is not observed during sputtering at room temperature. Ga solubility in In is good, so it is likely that the In islands contain Ga implanted from the ion beam. Growth of liquid In particles in the absence of sputtering has been observed, but only for substrate temperatures in the range of 500 to 800 °C. The In particles grew at arbitrary locations and adopted different shapes. After cooling to room temperature, it was shown that they had a crystalline structure independent on the orientation of the substrate [8].

Due to the ion distribution, preferential sputtering and topographical effects, the dots grow inside the pits sputtered by FIB, as schematically shown in Fig. 3. Therefore, their location can be controlled by FIB, as is shown in Fig. 4. The topography of a FIB-sputtered hole with low ion fluence was reported to be a depression or crater surrounded by a rim [9]. The rim is primarily due to a damaged or amorphous crystal structure, consisting of implanted Ga, interstitial atoms as well as vacancies, and, to a lesser extent, to redeposited material from the crater. This rim additionally constrains the growth of the islands to the crater. For InP, we expect only a small rim around the crater because simulations showed that amorphous InP is denser than crystalline InP [10]. As a consequence, InP as a substrate provides less control in growth as compared to materials with crystalline structure denser than the amorphous structure, namely Si.

In order to accelerate the coalescence of the dots, the substrate temperature was raised to 200 °C, ensuring that surplus In was liquid on the InP surface. The radius of the sputtered crater increases with increasing the ion fluence. The origin of this dependence is the ion distribution, as will be further discussed in Section 4. A consequence of this is less constrained growth of the islands; especially the location of larger islands is more difficult to control. A method to circumvent this dependency of island size and crater diameter is the growth of islands by adding material, which can be different from the substrate material, for example in molecular beam epitaxy or metal-organic chemical vapor deposition reactors [11]. We also milled V-shaped grooves at 200 °C and tried to fill them with liquid In to form nanowires. The mobility of In on InP however is low. This low mobility might be the result of subsurface growth of the nanodots [12]. Furthermore In, like Ga, has a large surface tension. Therefore, In prefers to build spheres rather than wires and does not diffuse to the bottom of the V-shaped trenches, even for substrate temperatures of 200 °C.

4 InI_3 nanodots and nanowires

InP is chemically attacked by molecular iodine (I_2). However, there's usually a protective natural oxide layer with a thickness of 1–2 nm that prevents this chemical reaction. During ion bombardment in vacuum, the oxide layer is sputtered away almost instantaneously due to its very high sputtering rate of 92 $\mu m^3/nC$, and iodine reacts spontaneously with InP and forms arbitrary shapes, such as the nanowire shown in Fig. 5. The main reaction products are PI_3 and InI_3, as measured by X-ray photoelectron spectroscopy. Additionally, iodine also reacts with implanted Ga to form GaI_3. From vapor pressure values, it can be concluded that GaI_3 and PI_3 desorb spontaneously for chamber pressures in the 10^{-6} mbar range. InI_3 however has a lower vapor pressure and remains on the InP surface at room temperature. The structure of InI_3 is initially amorphous. However, by heating 10 minutes at 160 °C in air, InI_3 rearranges to adopt its monoclinic crystal structure (Fig. 6).

The fact that the reaction is limited to areas previously irradiated by the ion beam opens the possibility to fabricate structures consisting of InI_3 by using the native oxide as a patterning mask. Analogous to e-beam lithography, the ion beam was used to write arbitrary patterns into InP, for instance lines in Fig. 7 and dots in Fig. 8. The ion fluence was varied from 0.008 pC per pixel to 20 pC per pixel. One line consisted of 238 pixels, spaced such as to achieve a beam overlap of 50%.

After ion irradiation, a nozzle was inserted into the vacuum chamber 150 μm above the InP surface and gaseous, molecular iodine was inserted into the vacuum chamber through the nozzle. The areas previously exposed to Ga^+ ions and thus cleared from the native oxide reacted to form InI_3. Diameters of these wires and dots depend on the dimensions of the initial pattern, especially on the ion fluence and beam shape. Larger ion fluences create deep V-shaped grooves and a lot of excess In that afterwards reacts with iodine. V-shaped grooves occur due to ion-trenching, a process where Ga ions with grazing incidence are backscattered from the sidewalls, especially likely when they hit a heavier In atom, as well as redeposition of sputtered material in the trench. As discussed in the previous section, there exists a trade-off between the available quantity of In and the minimum diameter of the structure. Wires with diameters below 100 nm and dots with diameters below 50 nm could be grown and observed with SEM. Dot diameter increased with increasing ion fluence, as shown in Fig. 8, and size distribution was homogeneous. For ion fluences above 0.05 pC per pixel, the areas covered with InI_3 merge, as is shown in the left inset of Fig. 7. Due to the ion distribution, areas outside the main exposure area are irradiated and the native oxide is sputtered as well, as will be discussed in more detail in Section 4. Therefore, these

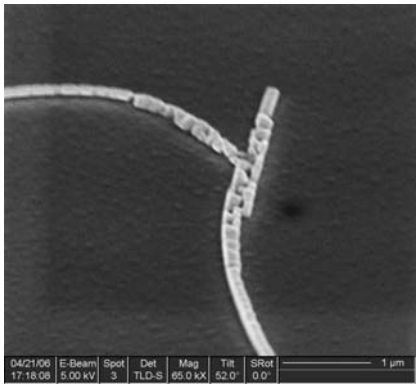

Fig. 5 SEM picture of an InI_3 nanowire grown spontaneously on an InP area previously irradiated with FIB and subsequently exposed to I_2. The nanowire adopts a random shape with respect to the ion beam scanning on the irradiated area.

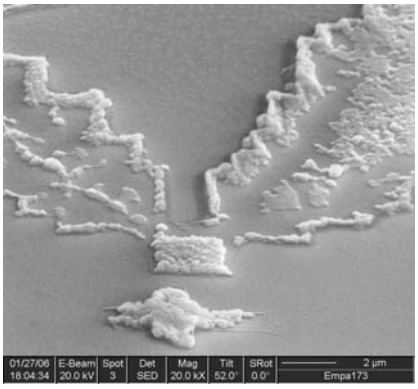

Fig. 6 SEM micrograph showing that InI_3 rearranges after heating 10 minutes at 160 °C on air, adopting its monoclinic crystal structure.

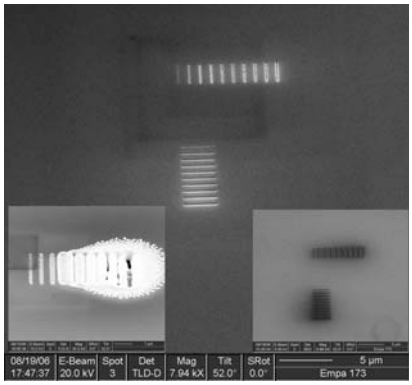

Fig. 7 SEM pictures demonstrating that InI_3 wires could be grown on previously irradiated areas at room temperature. Left inset shows overspray due to large ion fluence. Right inset shows areas after irradiation, prior to exposure to iodine. Fluence increases from left to right and top to bottom.

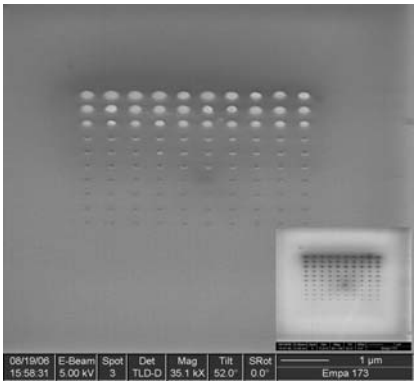

Fig. 8 SEM micrographs demonstrating that InI_3 dots could be grown on previously irradiated areas. Inset shows areas irradiated prior to exposition to iodine. Fluence increases from bottom to top and stays constant within one row.

areas also react with impinging iodine molecules, since iodine flux is constant over an area of $100 \times 100\ \mu m^2$.

5 Limitations

In dots smaller than 20 nm in diameter have been observed with AFM for the lowest ion fluences of 0.008 pC/pixel and are shown in Fig. 9. Direct observation of smaller structures using SEM is difficult due to the low difference in secondary electron yields between small In islands and the InP surface. AFM measurements are subject to particle contamination during the transfer from FIB to AFM in air and during AFM measurements.

There exists a fundamental limitation as to the density of dots that can be fabricated by FIB. This is due to the ion distribution constituting the ion beam. This distribution is known to be Gaussian in the

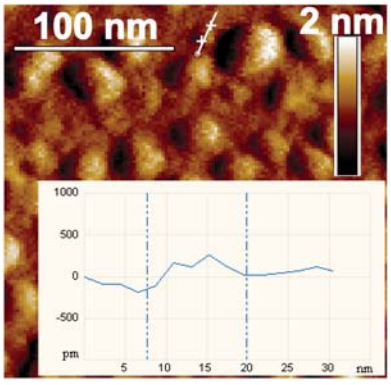

Fig. 9 (online colour at: www.pss-a.com) AFM picture showing that the smallest dot diameter is below 20 nm. The cross-section measurement is performed between the two crosses.

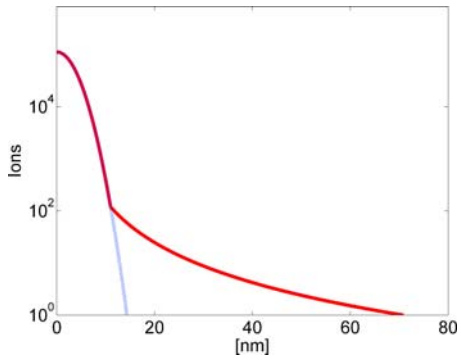

Fig. 10 (online colour at: www.pss-a.com) Gaussian beam shape (red) and Gaussian-Holtsmarkian distribution (blue). Ions impinge as far as 70 nm from the beam centre.

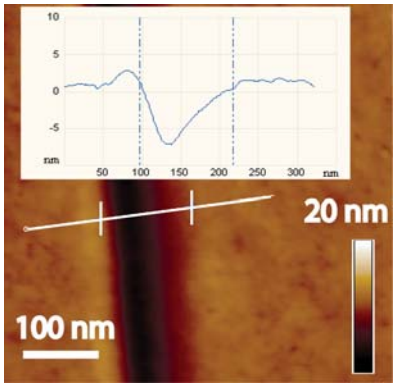

Fig. 11 (online colour at: www.pss-a.com) AFM picture and cross-section of a line sputtered in InP with a beam current of 1 pA (FWHM 7 nm). The line width is 120 nm. The ion fluence was 0.0025 pC/pixel and the beam overlap was 50%.

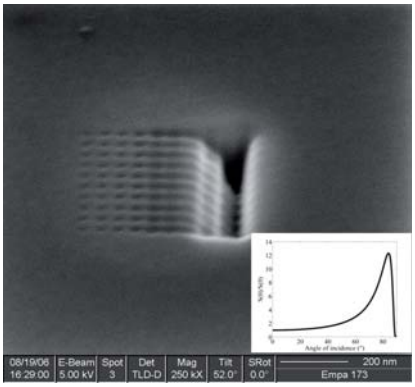

Fig. 12 SEM micrograph of a dot pattern with increasing ion fluence from left to right. Overlap of ion beam tails leads to sputtering of the area separating the dots, resulting in a trench. The inset shows a simulated sputter curve normalized to the sputter rate at normal incidence.

centre of the beam, but evolves into a Holtsmarkian-shape around three orders of magnitude below the peak intensity [13]. We have simulated such a beam shape for the lowest available current of 1 pA and a beam FWHM of 7 nm, as specified by the manufacturer under ideal operating conditions. From the simulation in Fig. 10, it clearly appears that ions impinge as far as 70 nm from the beam centre. For a purely Gaussian beam shape, no ions would impinge farther than 16 nm away from the beam centre. AFM measurement of cross-sections of a line sputtered at room temperature in InP using a finely focused 1.7 pA ion beam confirm the simulation results (Fig. 11). The fluence per pixel was 0.0025 pC and the beam overlap was 50%. The line width is 120 nm.

The sputtering rate of InP was determined to be 1.27 μm^3/nC for 30 keV Ga^+ and normal incidence. The amorphization threshold was reported to be around 1.6×10^{13} cm^{-2}, or 1 ion per 1600 $Å^2$ for InP [14]. Therefore, InP is particularly sensitive to ion irradiation. Increasing the ion fluence by either increasing the beam dwell time, rastering several times over the same area or by increasing the ion current, will gradually sputter the area separating individual structures due to the ions outside the central Gaussian beam. Individual dots merge to form lines and finally, deep trenches instead of well-separated dots are milled, as shown in Fig. 12. This effect is further enhanced by the increased sputter rate for non-normal incident ions, as the collision cascade moves closer to the surface and more atoms are sputtered, as is shown in the inset of Fig. 12, showing the sputter curve normalized to the sputter rate at normal incidence.

6 Conclusions

Localization and density of In-islands and InI_3 dots and wires can be controlled with FIB. Arbitrary 2D shapes can be written. The whole process occurs in the FIB-chamber. Important parameters are the beam shape, beam current, the irradiation time, the number of scan repetitions and the substrate temperature. Growth of In nanodots is intrinsic to the sputtering process and can also be applied for other compound materials, such as GaAs. Growth of InI_3 structures is a particularity of InP, since InI_3 has a low vapor pressure. The ultimate limitations of the surface density of dots and dot and wire size are determined by the substrate and native oxide sputter rates and the beam shape.

Acknowledgements V. Callegari wishes to thank Josef Kaufmann (EMPA, Abt. 135) for the AFM setup as well as the Office of Naval Research Science & Technology for the grant to attend the Trends in Nanotechnology (TNT 2006) conference and the CDM-INIT project of ETH Zurich for partial funding.

References

[1] S. Adachi, Physical Properties of III–V Semiconductor Compounds: InP, InAs, GaAs, GaP, InGaAs, and InGaAsP (Wiley-Interscience, New York, 1992).
[2] A. Lugstein et al., J. Vac. Sci. Technol. B **22**(6), 2995 (2004).
[3] J. B. Malherbe et al., Surf. Sci. **255**, 309 (1991).
[4] R. F. C. Farrow, J. Phys. D, Appl. Phys. **7**(17), 2436 (1974).
[5] P. Sigmund, Phys. Rev. **184**(2), 383 (1969).
[6] W. Ostwald, Z. Phys. Chem. **34**, 495 (1900).
[7] A. Lugstein et al., J. Vac. Sci. Technol. B **22**(3), 888 (2004).
[8] M. Gajdardziska-Josifovska et al., Surf. Sci. **340**, 141 (1995).
[9] A. Lugstein et al., Appl. Phys. A **76**, 545 (2003).
[10] L. J. Lewis et al., Phys. Rev. B **57**(3), 1594 (1998).
[11] A. Portavoce et al., Nanotechnology **17**, 4451 (2006).
[12] M. Gajdardziska-Josifovska et al., Surf. Rev. Lett. **4**(4), 655 (1997).
[13] J. W. Ward et al., J. Vac. Sci. Technol. B **6**(6), 2090 (1988).
[14] R. Menzel et al., J. Appl. Phys. **88**(10), 5658 (2000).